Large-Scale Structure and Individual Fingerprints of Locally Coupled Sleep Oscillations

Roy Cox[1,2,§], Dimitris S Mylonas[2,3,4], Dara S Manoach[2,3,4], Robert Stickgold[1,2]

1: Department of Psychiatry, Beth Israel Deaconess Medical Center, Boston MA, USA
2: Department of Psychiatry, Harvard Medical School, Boston MA, USA
3: Department of Psychiatry, Massachusetts General Hospital, Charlestown MA, USA
4: Athinoula A. Martinos Center for Biomedical Imaging, Charlestown MA, USA

§: Corresponding author: roycox.roycox@gmail.com

Abstract

The temporal coordination of slow oscillations and sleep spindles is believed to underlie processes of sleep-dependent memory consolidation and reorganization. Accumulating evidence of the predominantly local expression of these individual oscillatory rhythms suggests that their interaction may have a similar local component. However, it is unclear whether local coupling holds uniformly across the cortex, and whether and how these dynamics differ between fast and slow spindles, and sleep stages. Moreover, substantial individual variability in the expression of both spindles and slow oscillations raise the possibility that their cross-frequency interactions show similar individual differences. Using two nights of multi-channel electroencephalography recordings from 24 healthy individuals, we characterized the topography of slow oscillation-spindle coupling. We found that locally coupled oscillations occur over widespread cortical areas, but that their dynamics vary with spindle class, sleep stage, and location. Moreover, the phase of the slow oscillation cycle at which spindles were expressed differed markedly across individuals but was stable across nights. However, individual variability of coupling phase was not correlated with overnight memory change. These findings both add an important spatial aspect to our understanding of the temporal coupling of sleep oscillations and demonstrate the heterogeneity of coupling dynamics, which must be taken into account when formulating mechanistic accounts of sleep-related memory processing.

Introduction

During non-rapid eye movement (NREM) sleep, highly organized oscillatory rhythms of slow oscillations and sleep spindles occur across widespread brain areas. In recent years, these electroencephalographic (EEG) waveforms have attracted considerable attention, owing to their close relation with cognitive functioning (De Gennaro and Ferrara, 2003; Lüthi, 2013). Both spindles and slow oscillations (SOs) are closely linked to plasticity and memory processes (Marshall et al., 2006; Mölle et al., 2009; Barakat et al., 2011; Cox et al., 2012; Ngo et al., 2013), and their altered expression in aging and various neuropsychiatric disorders (Ferrarelli et al., 2007; Wamsley et al., 2012; Mander et al., 2013; Plante et al., 2013; Latreille et al., 2015; Helfrich et al., 2017) has made them therapeutic targets of considerable interest.

SOs are large-amplitude ~1 Hz neocortical oscillations of alternating depolarized and hyperpolarized brain states that modulate neuronal spiking (Steriade et al., 1993; Cash et al., 2009; Nir et al., 2011). Conversely, spindles are short (0.5–2 s) bursts of sigma band activity (9–16 Hz) initiated by the thalamus that propagate to cortex (Steriade et al., 1987). In humans, spindles can be classified as either slow (9–12.5 Hz) or fast (12.5–16 Hz; but see (Cox et al., 2017) for an overview of spectral definitions in use). Aside from their oscillatory frequency, fast and slow spindles differ in topography (Werth et al., 1997; Zeitlhofer et al., 1997), hemodynamic activity (Schabus et al., 2007), heritability (Purcell et al., 2017), and development (D'Atri et al., 2017). Moreover, spindles exhibit replicable individual differences in frequency (De Gennaro et al., 2005; Purcell et al., 2017) and topography (Cox et al., 2017), relating to underlying variability in neuroanatomy (Piantoni et al., 2013b).

Intriguingly, SOs and spindles are temporally coordinated, such that spindle activity preferentially occurs in a particular SO phase. While fast spindles tend to have maximal power around the depolarized SO peak, slow spindles have greatest intensity in the peak-to-trough transition (Mölle et al., 2011; Cox et al., 2014c; Klinzing et al., 2016; Yordanova et al., 2017). Moreover, this phenomenon of cross-frequency coupling (Canolty and Knight, 2010) has been tied to sleep-dependent memory consolidation, such that appropriate spindle timing relative to the SO phase enhances memory (Niknazar et al., 2015; Demanuele et al., 2017; Helfrich et al., 2017; Latchoumane et al., 2017).

While both SOs and spindles are found across widespread cortical regions, they are more often local (i.e., restricted in spatial extent) than global events (Massimini et al., 2004; Andrillon et al., 2011; Nir et al., 2011; Piantoni et al., 2016), thereby providing a potential mechanism for circuit-specific plasticity and consolidation (Huber et al., 2004, 2006; Cox et al., 2014a; Yordanova et al., 2017). Accordingly, locally detected SOs coordinate spindles in a spatially restricted fashion (Cox et al., 2014c). However, as previous studies have focused on either global SOs, or SOs detected at a restricted number of scalp sites, the spatial extent of local SO-spindle coupling and its

compatibility with regionally specific memory processing remain unknown. Moreover, assessing coupling dynamics separately for fast and slow spindles, and for deep N3 and light N2 NREM sleep, could shed light on the functional role of these different spindle classes and sleep stages. Finally, observations of reproducible individual differences in the expression of spindles, as well as SOs (Massimini et al., 2004), raise the possibility that SO-spindle coupling dynamics show similar individual differences.

Here, we demonstrate that local SOs coordinate local spindle activity across the scalp, but with important variations depending on spindle class, sleep stage, and cortical region. Moreover, we observed marked individual differences in the precise SO phase at which spindle activity preferentially occurs. Although this variability was not associated with overnight procedural memory improvement, it was highly stable across nights, indicating that coupling phase constitutes a stable trait that may have important functional and clinical implications.

Materials and Methods

Protocol and participants

The present study describes novel analyses of full-night EEG data that we reported on previously (Cox et al., 2017). Twenty-four healthy individuals (age: 30.2 ± 6.3; 18 male, 6 female) gave written informed consent in accordance with the Declaration of Helsinki and were paid for participation. Data were acquired as part of a double-blind, placebo-controlled, cross-over study of eszopiclone in schizophrenia patients. Only the two consecutive placebo nights are considered in the present study. The study was approved by the Partners Human Research Committee. Additional details regarding participant screening and the protocol can be found in our previous report (Cox et al., 2017).

Finger tapping Motor Sequence Task

After an initial a baseline night, on the second night participants performed the finger tapping Motor Sequence Task (MST), a well-validated probe of sleep-dependent memory consolidation (Walker et al., 2002; Manoach et al., 2004; Fischer et al., 2005; Wamsley et al., 2013; Demanuele et al., 2017). Subjects were trained on the MST 2 h 45 m prior to bedtime, and tested 1 h after awakening. The MST involves pressing four numerically labeled keys on a standard computer keyboard with the fingers of the left hand, repeating a five-element sequence (4-1-3-2-4) "as quickly and accurately as possible" for 30 seconds. The numeric sequence was displayed at the top of the screen, and dots appeared beneath it with each keystroke. During both training and test sessions, participants alternated tapping and resting for 30 seconds for a total of 12 tapping trials. The outcome measure was the number of correct sequences per trial, which reflects both the speed and accuracy of performance. Overnight improvement was calculated as the percent increase in correct sequences from the last three training trials to the first three test trials the following morning (Walker et al., 2002).

Data acquisition and preprocessing

Polysomnography was collected using 62-channel EEG caps (Easycap GmbH, Herrsching, Germany) with channel positions in accordance with the 10-20 system. Additional EEG electrodes were placed on the mastoid processes, and on the forehead as online reference. Electrooculography and bipolar chin electromyography were monitored as well. An AURA-LTM64 amplifier and TWin software were used for data acquisition (Grass Technologies). Impedances were kept below 25 kΩ and data were sampled at 400 Hz with hardware high-pass and low-pass filters at 0.1 and 133 Hz, respectively.

Sleep staging was performed in TWin using a limited number of channels with a contralateral mastoid reference on 30 s epochs according to standard criteria (Iber et al., 2007). Initial processing of multi-channel EEG data was performed in BrainVision Analyzer 2.0 (BrainProducts, Germany). All EEG channels were band-pass filtered between 0.3 and 35 Hz and notch filtered at 60 Hz. Channels displaying significant

artifacts for more than 30 minutes of the recording were interpolated with spherical splines. EEG data were then re-referenced to the average of all EEG channels. Upon visual inspection, epochs containing artifacts were removed. To remove cardiac artifacts we used independent component analysis with the Infomax algorithm (Makeig et al., 1997). For each night and individual, remaining epochs were concatenated separately for sleep stages N3 and N2, resulting in 80.2 ± 39.5 (mean ± SD) and 82.3 ± 28.7 min of available N3 for the two nights, and 174.4 ± 60.1 and 211.4 ± 52.4 min of N2.

All subsequent processing and analysis steps were performed in Matlab (the Mathworks, Natick, MA), using custom routines and several freely available toolboxes including EEGlab (Delorme and Makeig, 2004) and the CircStat toolbox for circular statistics (Berens, 2009). After removal of non-EEG channels and the mastoids, leaving 58 channels for analysis, we applied a surface Laplacian filter to each record to minimize the impact of volume conduction and thereby highlight local cortical processing (Perrin et al., 1989; Tenke and Kayser, 2005).

SO detection

Individual SOs were detected during N3 and N2 on each channel using an established method closely resembling our previous approach (Cox et al., 2014c). Specifically, the Laplacian-filtered signal of each channel was band-pass filtered between 0.4 and 1.5 Hz (zero-phase shift, third-order IIR filter). An SO was detected when (1) the latency between subsequent negative and positive zero-crossings of the filtered trace fell between 0.3 and 0.75 s, (2) the negative half-wave reached a minimum of –1 $\mu V/cm^2$, (3) the amplitude difference between the trough and the subsequent local maximum exceeded 2 $\mu V/cm^2$, and (4) the unfiltered EEG amplitude difference between the time points corresponding to the Laplacian-based SO trough and peak exceeded 50 µV. This final criterion ensures that Laplacian-detected SOs correspond to similar fluctuations in the regular EEG. The only difference from our previous report concerns the precise Laplacian and EEG amplitude criteria, which were relaxed here to detect events in regions where SO-band amplitude fluctuations are of smaller amplitude than in frontal areas, where SOs are conventionally detected. We marked SOs as 2 s time windows centered on each trough (1 s on either side) to capture at least one full cycle of the oscillation. Note that while this procedure allows for overlapping time windows between closely spaced SOs, the number of detected SOs per minute (see Results) suggests this occurred infrequently.

Time-frequency power

To assess how local SOs modulate faster activity across an extended frequency range, we performed single-subject time-frequency analyses centered on each channel's SO troughs. Window size was set to ± 1.5 s around each SO trough to avoid edge artifacts stemming from the convolution. Decomposition was performed with a family of complex Morlet wavelets, according to $e^{i2\pi tf}e^{-t^2/(2\sigma^2)}$, where i is the imaginary operator, t is time, f is frequency (30 logarithmically spaced frequencies between 5 and 25 Hz), and σ is the wavelet width. We defined the width σ as $\lambda/(2\pi f)$, where λ is the

number of wavelet cycles, which was set to 5. The resulting time-frequency representations were down-sampled to 100 Hz to reduce the amount of data. Power was defined as the squared magnitude of the convolution result. Power estimates at each time point in each SO window were converted to percentage change relative to average power from –1 to 1 s surrounding the SO trough (i.e., single-trial baseline). This normalization ensures that power values can be compared across frequencies and channels. Time-frequency spectrograms were averaged across all SO windows for each channel.

SO co-occurrences

We determined the degree to which SOs detected on a "source channel" were also observed on a "target channel". Specifically, for each subject, source channel, and SO, a co-occurrence was counted when a target channel (excluding the source channel itself) expressed an SO trough within a fixed window of either ±400 or ±100 ms surrounding the source SO trough. Target channel counts were averaged across SOs to obtain a measure of average channel involvement for each source channel. In a complementary approach, we determined, for each subject and source channel, the relative proportion of source SOs that were detected at each possible number of target channels (ranging from 1 to 57). These normalized histograms were subsequently averaged over subjects, and the resulting group-level histograms were converted to cumulative distributions to determine the maximum number of target channels engaged for 50, 75, and 99% of source SOs.

SO-spindle coupling

We obtained estimates of both SO-spindle coupling strength and coupling phase (defined below) for each subject, night, sleep stage, spindle class, and electrode. We first filtered the Laplacian-transformed multi-channel data in the canonical SO range (0.5–2 Hz), and in 1.3 Hz wide windows centered on each subject's individual fast and slow sigma frequencies. Individualized sigma frequencies were determined using a spatial filtering approach based on generalized eigendecomposition, as described in our previous report (Cox et al., 2017). We used the Hilbert transform to obtain the analytic signal of each channel in each frequency band, and extracted the instantaneous phase of the SO signals and the instantaneous amplitudes of the fast and slow sigma signals at every time point. Instantaneous amplitudes were squared to obtain power envelopes. Then, for all three time series (SO phase, fast and slow sigma power), we extracted the previously identified 2 s windows surrounding each SO trough and concatenated them into segments of 20 SOs, corresponding to 40 s. In case the number of detected SOs was not divisible by 20, the incomplete final segment was padded with SOs randomly resampled from (the same) final segment. The segmentation step was performed to ensure that permutation-based z-scoring (see below) was performed on data segments of identical length, thus avoiding confounds due to differences in number of detected SOs.

We determined phase-amplitude coupling for each segment of 20 concatenated SOs using an adaptation of the mean vector length method (Canolty et al., 2006) that adjusts for possible bias stemming from non-sinusoidal shapes of the modulating frequency (van Driel et al., 2015). Specifically, complex-valued debiased phase-amplitude coupling (dPAC) was calculated as:

$$\mathrm{dPAC} = \frac{1}{n}\sum_{t=1}^{n}(SIG_{pow}(t) * (e^{iSO_{phase}(t)} - B))$$

where *i* is the imaginary operator, *t* is time, $SIG_{pow}(t)$ and $SO_{phase}(t)$ are the sigma power and SO phase time series, and *B* is the mean phase bias:

$$B = \frac{1}{n}\Sigma_{t=1}^{n} e^{iSO_{phase}(t)}$$

Raw coupling strength (i.e., the degree to which sigma power is non-uniformly distributed across the SO cycle) was defined for each segment as the magnitude (i.e., length) of the mean complex vector. Under the null-hypothesis of no systematic SO-spindle coupling, vectors of different length should be randomly distributed over SO phases, resulting in a mean vector length close to zero. However, if longer vectors preferentially occur in a particular phase range, the mean vector length will deviate substantially from zero, signaling SO-spindle coupling. Importantly, absolute coupling strength depends on absolute sigma power. Thus, differences in sigma power between electrodes, spindle classes, sleep stages, and individuals, which we have described in detail elsewhere (Cox et al., 2017), confound the interpretation of this measure. Therefore, for every segment and channel, we constructed a surrogate distribution of coupling strengths by repeatedly (n=1,000) shuffling the SO phase time series with respect to the sigma power time series, and recalculating the mean vector length for each iteration. We then z-scored the observed coupling strength with respect to this null distribution of coupling strength values, and averaged z-scores across segments. Thus, the z-scored measure ($dPAC_Z$) indicates how far, in terms of standard deviations, the observed coupling estimate is removed from the average coupling estimate under the null hypothesis of no coupling. Coupling phase (i.e., the SO phase of maximal sigma power) was defined as the phase angle of the (unnormalized) mean complex vector, averaged across segments.

Experimental Design and Statistical Analysis

We analyzed 58-channel EEG data from 24 healthy volunteers across two consecutive full nights of sleep. While we analyzed both nights, we report analyses from the baseline night, except for cross-night comparisons, and analyses involving memory performance, for which the learning night was used.

To assess whether coupling strength deviates from chance levels, we compared $dPAC_Z$ values to zero with one-sample t-tests. For within-subject comparisons of linear

outcome variables (e.g., N3 vs. N2 coupling strength), we used paired-sample t tests. The circular Rayleigh test was used to determine whether circular coupling phase distributions deviate from uniformity. For within-subject comparisons of circular distributions (e.g., N3 vs. N2 coupling phase), we calculated phase differences (wrapped to the –180 to +180 interval) and used a one-sample t-test to compare differences to zero. Associations of coupling phase across nights were assessed using circular-circular correlations, while associations of coupling phase and behavior were tested using circular-linear correlations. Significance of time-frequency power modulations was assessed by performing a one-sample t-test vs. zero at each time-frequency bin. All statistical tests are two-sided, unless stated otherwise. Correction for multiple tests was performed with the False Discovery Rate procedure (Benjamini and Hochberg, 1995).

Results

Local dynamics of sleep oscillations

We analyzed two nights of 58-channel EEG data from 24 healthy volunteers. After applying a surface Laplacian spatial filter to emphasize local neural dynamics (Perrin et al., 1989; Tenke and Kayser, 2005), we detected SOs on each electrode in both N3 and N2 NREM sleep. Fig. 1A shows a single subject's raw and SO-filtered Laplacian traces for five channels – AFz, FCz, CPz, POz, C6 – at the same time interval, with detected SOs indicated. Sizable channel differences in the SO-filtered traces and their detected SOs are visible, consistent with the notion that most SOs are local phenomena. Similarly, slow and fast sigma activity showed notable differences between channels, indicating that spindle dynamics, like SOs, show regional variability. Substantial within-channel differences in the time courses of slow and fast sigma are also apparent, suggesting that the two sigma bands reflect different neuronal dynamics. This clear evidence of regional variation within spindle and SO frequency bands motivated us to examine channel-specific SO-spindle coupling.

To illustrate local SO-spindle coupling for this sample subject using conventional techniques, we time-locked each sample channel's raw Laplacian time series to that channel's identified SO troughs, allowing us to evaluate time-frequency power in the 5–25 Hz range as a function of the SO waveform. This revealed significant modulations of faster activity on each sample channel (Fig. 1B), similar to previous reports detecting global (Mölle et al., 2011; Klinzing et al., 2016) or local SOs (Cox et al., 2014c). Specifically, we found robust increases in ~15 Hz fast sigma power, extending to higher frequencies, centered on the SO peaks preceding and following the SO trough, while fast sigma was suppressed in the SO trough. In contrast, activity in the slow sigma and theta range (~5–10 Hz) was markedly enhanced prior to the SO trough, but suppressed in the SO peaks preceding and following the SO trough. Similar observations were made for the majority of channels and subjects. Thus, despite different temporal dynamics of SO and sigma activity on different channels, the relation between local SO phase and local sigma power appears to remain intact.

While this time-frequency approach demonstrates local coupling, this method suffers from limited temporal and spectral precision. It cannot specify the precise SO phase at which activity in the fast and slow sigma ranges peaks, necessitating alternative approaches, as described below.

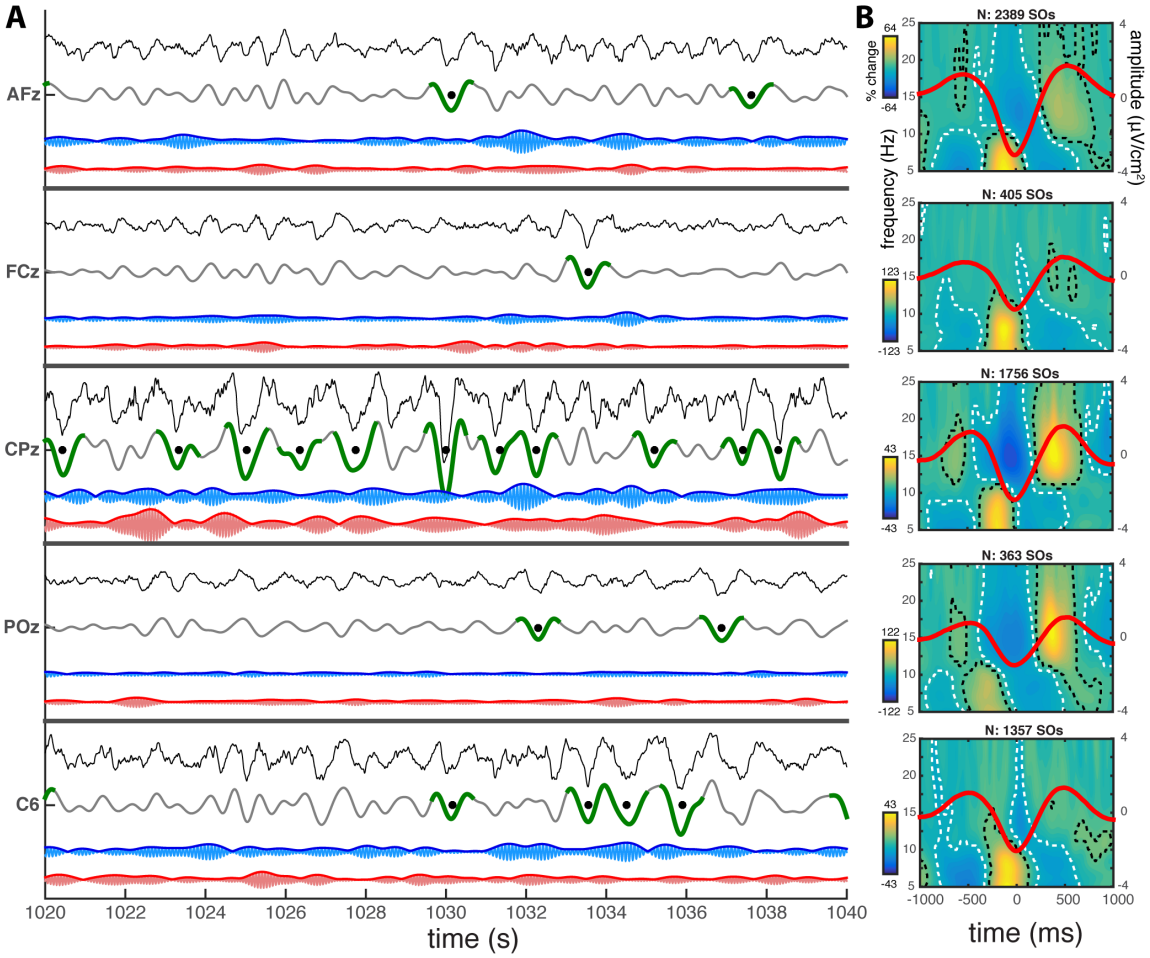

Figure 1. Regional variations in SO, slow spindle, and fast spindle activity. (A) Twenty second excerpt of single subject's N3 sleep for five channels – AFz, FCz, CPz, POz, C6 showing, from top to bottom, the raw Laplacian EEG (black), SO- (gray), slow sigma- (blue), and fast sigma-filtered (red) traces. Detected SOs are shown in green (trough ± 500 ms), with the troughs marked with black dots. Sigma traces were multiplied by a factor 6 for visualization purposes. (B) Same subject's time-frequency spectrograms time-locked to SO troughs (average SO waveforms superimposed in red; total number of detected SOs above spectrogram). Activity (percentage power change relative to baseline; see Materials and Methods) in the slow sigma/theta and fast sigma ranges is modulated by SOs on each channel, as signified by clusters of significant power increases and decreases (indicated by black and white dashed outlines, respectively). Significance was assessed by performing a one-sample t-test vs. zero at each time-frequency bin, followed by False Discovery Rate correction for multiple comparisons (P_{corr}<0.05).

SO characteristics

Overall, across subjects and sleep stages on Night 1, we detected 753,641 SOs. Although subjects spent significantly less time in N3 than N2 (80.2 ± 39.5 min vs. 174.4 ± 60.1, paired t(23)=6.0, $P<10^{-5}$), almost four times as many SOs were detected in N3 as in N2 (20,089 ± 19,232 vs. 5,729 ± 4,943, t(23)=3.9, P<0.001). Corresponding channel-averaged SO densities (number per minute) showed a similarly significant six-fold sleep stage difference (N3: 2.4 ± 1.5; N2: 0.4 ± 0.3; t(23)=7.0, $P<10^{-6}$). Topographical

examinations (Fig. 2A) confirmed this stage difference while also revealing known regional differences in the prevalence of SOs, with markedly higher SO densities over anterior and central electrodes than in temporal and posterior areas (Kurth et al., 2010). Trough-to-peak SO amplitudes were greatest at frontal electrodes, but relatively uniform over the rest of the scalp (Fig. 2B). Averaged across electrodes, SOs were of slightly but significantly larger amplitude in N3 (2.84 ± 0.26 μV/cm^2) relative to N2 (2.76 ± 0.22 μV/cm^2; t(23)=2.2, P=0.04).

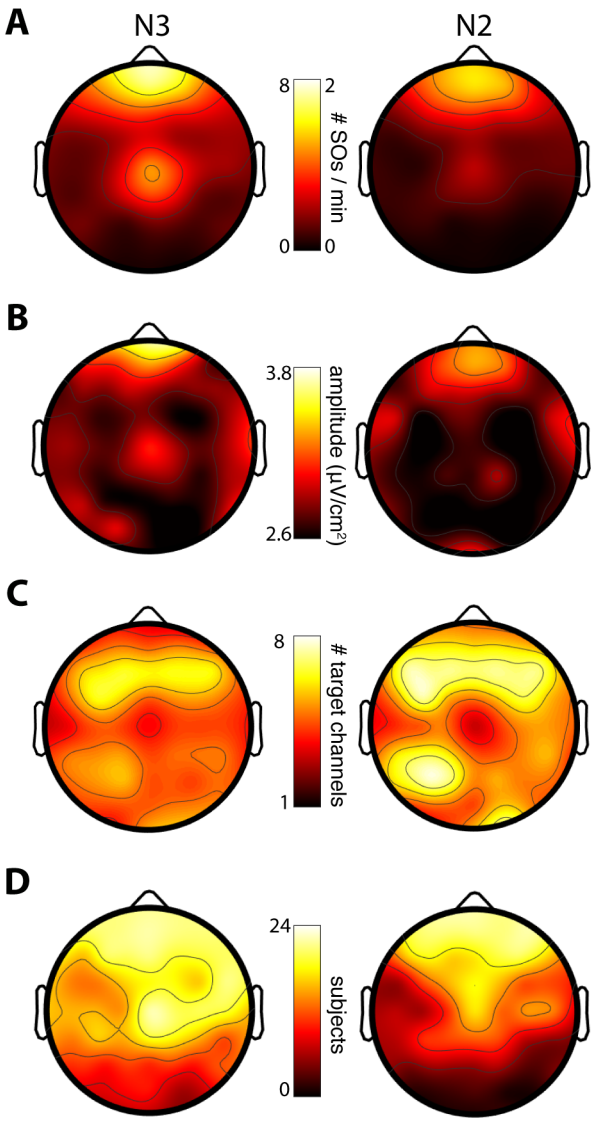

Figure 2. Topographical distributions of slow oscillations in N3 and N2. (A) SO densities (number/minute). Note the different scales for N3 and N2 SO density. (B) SO amplitudes (trough-to-peak). (C) Average number of target channels with an SO trough co-occurring within 100 ms surrounding the SO trough of a source channel. (D) Number of subjects included.

SO co-occurrences

To formally assess the degree to which SOs are local, we determined the number of "target" channels that showed SOs co-occurring with each SO detected on a "source" channel. We counted a co-occurrence when the SO trough of a target channel occurred within a fixed window surrounding the source SO trough. Using a liberal window of ± 400 ms on either side (Nir et al., 2011), we found that SOs involved fewer than 10 channels on average (mean number of target channels across source channels, averaged across SOs and subjects; N3: 8.6 ± 1.3; N2: 9.4 ± 1.5), indicating that most detected SOs engage only a limited number of electrodes. Despite their large difference in SO densities, N3 and N2 SOs showed very similar numbers of co-occurring channels, although channel involvement was significantly higher in N2 than N3 ($t(57)=5.6$, $P<10^{-6}$).

Next, we narrowed the window of co-occurrence to ± 100 ms in order to count only co-occurrences where SOs showed minimal phase shifts across channels. This led to a 40-45% reduction in the average number of channels participating in each SO, leaving 4.9 ± 0.9 and 5.7 ± 1.2 involved channels in N3 and N2, respectively (paired t-tests for wide vs. narrow window: both $t(57)>22.2$, $P<10^{-29}$; stage difference: $t(57)=9.0$, $P<10^{-11}$). In other words, only roughly half of target-channel SOs occurring in conjunction with a source SO were approximately in phase with the source SO. Further topographical examinations (Fig. 2C) using this restricted window width indicated greatest co-occurrence for SOs detected in anterior source channels, with this hotspot shifted slightly posteriorly relative to the sites with highest SO density and amplitude.

The preceding analyses are based on mean channel involvement averaged across all SOs detected in each source channel. We next examined the number of involved channels across individual SOs (using the restricted 100 ms window). Normalized histograms for two sample channels, averaged across subjects, illustrate the skewedness of these distributions, with the majority of SOs affecting only a minority of channels, with the modal number of channels involved being only 1 and 2 (Fig. 3). Across source channels, the modal number of target channels ranged between 1 and 11 (N3: 2.7 ± 1.7; N2: 2.6 ± 1.9; $t(57)=0.4$, $P=0.69$), with greatest channel involvement again seen for frontal source channels. Moreover, cumulative distributions indicated that, on average across source channels, 50% of SOs involved no more than 10% of channels (mean number of target channels for N3: 4.3 ± 0.9; N2: 5.0 ± 1.5; $t(57)=4.7$, $P<10^{-4}$). Moreover, 75% of all SOs were detected in no more than 15% of channels (N3: 7.3 ± 1.1; N2: 8.7 ± 2.2; $t(57)=6.2$, $P<10^{-7}$), and less than 1% of SOs involved more than a third (99th %ile – N3: 15.9 ± 1.5; N2: 18.6 ± 2.6; $t(57)=8.6$, $P<10^{-11}$). Across subjects, nights, and sleep stages, the single-most widespread SO recruited only 31 (54%) of target channels. In sum, this pattern of results, which was reproducible across nights, indicates that SOs are overwhelmingly local in nature (especially in N3).

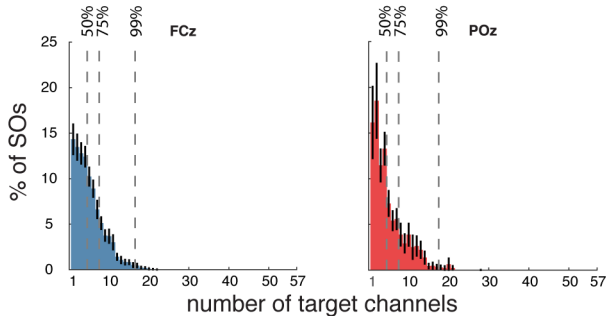

Figure 3. Distribution of SO involvement (percentage of individual source SOs detected on a given number of target channels). Mean ± SEM (black error bars) across subjects for N3 SOs detected on anterior (FCz) and posterior (POz) source channels. Vertical dashed lines indicate channel count where cumulative distribution contains 50, 75, and 99% of SOs. Distributions were qualitatively similar for all channels and sleep stages.

There were substantial individual differences in the number and density of detected SOs, with some subjects expressing few or no SOs meeting our detection criteria on one or more channels. To attain reliable estimates of SO-spindle coupling in subsequent analyses, we included, for each electrode, only those subjects showing a minimum of 20 detected SOs (evaluated separately for N3 and N2). Using this criterion, we included an average of 16.0 ± 5.1 subjects per electrode (range: 5–23) in N3, and 11.1 ± 7.1 (range: 1–23) in N2. Conversely, we included 38.8 ± 14.1 electrodes per subject (range: 4–57) in N3, and 26.8 ± 12.6 (range: 11–56) in N2. Fig. 2D displays the number of subjects included at each electrode, showing reduced inclusion rates over posterior areas, especially during N2.

SO-spindle coupling

To determine cross-frequency coupling between locally detected SOs and local spindle activity we employed the debiased phase-amplitude coupling (dPAC) approach (van Driel et al., 2015). The dPAC method provides information on both coupling strength (i.e., the degree to which sigma activity is non-uniformly distributed across the SO cycle), and coupling phase (i.e., the SO phase of maximal sigma activity). Using this method, we determined SO-spindle coupling at each electrode, separately for N3 and N2 sleep, and separately for fast and slow sigma activity. Fast and slow sigma ranges were set for each individual based on their own power spectrum (fast sigma: 13.5 ± 0.6 Hz; slow sigma: 10.9 ± 0.7 Hz), thereby targeting spindle activity in a subject-specific manner (Cox et al., 2017). We further normalized coupling strengths using a permutation-based reshuffling approach, resulting in z-scored coupling strengths ($dPAC_Z$). Critically, this normalized measure of coupling strength is independent of absolute sigma power and is therefore not influenced by potential differences in sigma power between electrodes, sleep stages, or individuals (see Materials and Methods).

Local SOs coordinate local spindle activity across the scalp

We first sought to determine the presence of SO-spindle coupling (i.e., above-zero coupling strengths), irrespective of coupling phase. We did this separately for each

combination of fast/slow spindles and N2/N3 sleep (henceforth: conditions). In a first step, we averaged coupling strengths across subjects for each electrode. Average channel coupling strengths were significantly greater than zero in each condition (all t(57)>39.2, $P<10^{-42}$). Although absolute differences were small, coupling was significantly stronger in N3 than N2 for fast sigma, while significantly weaker for slow sigma (Table 1). Coupling strengths were also significantly greater for fast than slow sigma in N3, but not different in N2.

	N3	N2	t(57)	P
fast	29.2 ± 5.1	25.7 ± 5.0	4.8	$<10^{-4}$
slow	23.5 ± 2.3	26.2 ± 3.9	4.7	$<10^{-4}$
t(57)	7.7	0.6		
P	$<10^{-9}$	0.55		

Table 1. Mean (± SD) coupling strengths ($dPAC_Z$) in each condition and statistical results from paired t-tests.

To assess the spatial extent of this SO-spindle coupling, we next analyzed coupling strengths separately for each electrode. Correcting for multiple comparisons with the False Discovery Rate (FDR) procedure (Benjamini and Hochberg, 1995), all 58 electrodes showed significant ($P_{corr}<0.05$) SO-spindle coupling during N3 for both fast and slow sigma, while 52 of 58 (fast) and 51 of 58 (slow) electrodes reached significance for N2. The few electrodes not reaching significance were exclusively positioned over posterior regions with low numbers of both SOs and included subjects.

We further assessed the proportion of included (≥ 20 SOs) subject-electrodes that exhibited evidence of SO-spindle coupling, operationalized as $dPAC_Z$ values > 1.65 (corresponding to one-sided P<0.05, uncorrected). Across N3 (*n* = 930) and N2 (*n* = 642), all 3,144 subject-electrode-condition combinations showed significant coupling except for a single subject-electrode that failed to reach significance for fast spindle coupling during N3 (99.97%). Highly similar results were found for Night 2. These analyses confirm the robustness of SO-spindle coupling at all scalp sites, for both fast and slow spindles, and in both N3 and N2 sleep.

Local coupling phase depends on spindle class and sleep stage

Given this widespread coupling of local spindle activity to local SOs, we turned to topographical analyses of coupling phase (i.e., the SO phase at which sigma activity is greatest). For fast spindles, activity was preferentially expressed on the rising slope of the SO in both N3 (group averages across electrodes: 50 ± 29°; Fig. 4A) and N2 (80 ± 33°; Fig. 4B; see below for direct stage comparisons). Phase distributions across channels were highly non-uniform (Rayleigh test: both $P<10^{-22}$; see dashed insets), reflecting the consistency of coupling phases across the scalp. To assess the consistency of coupling phases across subjects, we examined, for each electrode, whether coupling phases were non-uniformly distributed. Right panels of Fig. 4AB shows these distributions for the five

sample channels, and indicate tight group-level phase clustering before the SO peak on most channels (although clear between-subject differences are evident even for the most consistent electrodes; see below). Across the scalp, 46/58 (N3; uncorrected: 49/58) and 26/58 (N2; uncorrected: 32/58) electrodes showed significantly non-uniform distributions of coupling phase, indicating highly consistent group effects over much of the scalp (significant electrodes indicated on topographies as green circles). The failure of most posterior channels to reach significance is most like due to the small number of subjects, particularly in N2, with sufficient numbers of SOs to be included in the analysis.

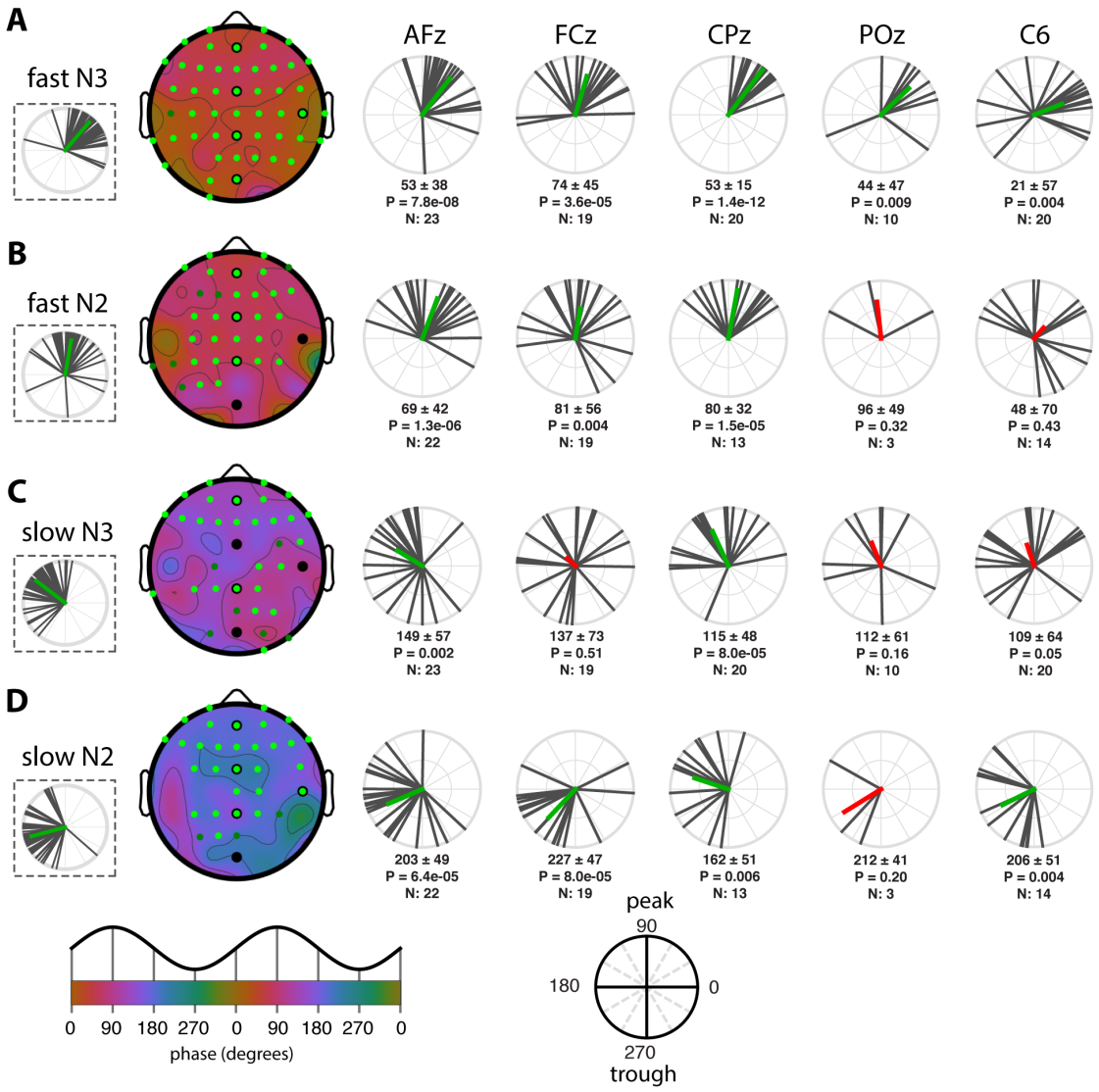

Figure 4. SO-spindle coupling phases across the scalp and individuals. (A) fast N3 spindles. (B) fast N2 spindles. (C) slow N3 spindles. (D) slow N2 spindles. **Left:** topographies of mean preferred coupling phase across individuals, with dashed insets on the left showing circular distributions across channels (black vectors: individual channels, averaged across individuals; green vectors: channel averages). Green colored circles on topographical maps indicate electrodes showing significantly non-uniform phase distributions across subjects after correcting

for multiple comparisons (bright green) or uncorrected (dark green). Black circles indicate selected electrodes plotted on the right. **Right:** circular plots display phase distributions across individuals (black). Subject-average vectors (colored) indicate both average phase and cross-subject consistency, expressed as its length. Numbers below each circular plot indicate mean phase (± SD), P value (uncorrected) of Rayleigh tests for non-uniformity, and number of included subjects. Mean vector is colored green when the uncorrected P is <0.05, and red otherwise. Bottom insets indicate mapping from phases to topographical color map and circular plots.

Next, we asked whether fast spindle activity peaked in different SO phases in N2 and N3 by calculating within-subject N2-N3 phase differences at each electrode, and comparing these to zero. (Subjects are included only if they have ≥ 20 SOs in both N2 and N3.) Across the scalp, averaged within-subject N2-N3 coupling-phase differences were significantly different from zero (15 ± 37°; t(57)=2.5, P=0.02), with fast spindles occurring slightly later in N2 than N3. (This estimate of within-subject phase difference differs from the 30° difference seen above for calculations of group averages across electrodes.) This small (15°) difference in preferred coupling phase, together with the fact that no individual electrode showed a significant N2-N3 difference after multiple comparison correction (uncorrected: 8/58), lead us to conclude that the organization of fast spindle activity by SOs does not differ importantly between these sleep stages.

Slow spindles were organized by SOs quite differently than fast spindles, showing maximal activity in the transition from the SO peak to the trough (group averages across electrodes: N3: 143 ± 30°, Fig 4C; N2: 195 ± 34°, Fig. 4D). As for fast spindles, phase distributions were highly non-uniform (Rayleigh: N3 and N2, both $P<10^{-21}$), indicating that slow spindles are preferentially expressed in similar SO phases across the scalp in both N3 and N2. Examining cross-subject consistency, we found that 27/58 (N3; uncorrected: 33/58) and 29/58 (N2; uncorrected: 32/58) electrodes showed significantly non-uniform phase distributions across subjects, with anterior regions expressing this most consistently across sleep stages. Although indicative of consistent group-level clustering over much of the scalp, these findings and the circular distributions of Fig. 4CD indicate that between-subject variability of coupling phases is generally greater for slow than fast spindle activity.

Examining N2-N3 stage differences for slow-spindle coupling, we found that within-subject phase differences were significantly different from zero (group average across electrodes: 48 ± 37°; t(57)=9.0, $P<10^{-11}$), with the phase of maximal slow-spindle coupling about 45° later in N2. Testing of individual electrodes followed by multiple comparison correction revealed that of the 58 electrodes, only 12 (uncorrected: 14) electrodes (7 anterior, 5 central) had significantly different coupling angles in N3 compared to N2 (e.g., circular distributions of AFz in Fig. 4CD).

Finally, we directly compared the preferred coupling phases of fast and slow spindles. Within-subject fast-slow phase differences were significant in both N3 (group average across electrodes: fast - slow = –80 ± 42°; t(57)=7.0, $P<10^{-8}$; Fig. 5A) and N2 (–

114 ± 45°, t(57)=–6.2, $P<10^{-7}$; Fig. 5B), indicating that maximal fast spindle activity occurs about a quarter of a cycle earlier than for slow spindles. The larger phase difference in N2 is consistent with the aforementioned observation of slow spindles being phase-delayed in N2 relative to N3. On an electrode-by-electrode basis, fast-slow differences were confirmed statistically for 17/58 electrodes in N3, and 2/58 in N2 using the most stringent correction for multiple comparisons (Fig. 5, green circles). However, using an uncorrected threshold of P<0.05 increased the channel count to 22 of 58 in N3 and 18 of 58 in N2 (Fig. 5, green + white circles). In sum, these findings indicate that fast spindle activity is expressed distinctly earlier in the SO cycle than is slow spindle activity, and that this phenomenon can be observed across widespread cortical regions, particularly during N3.

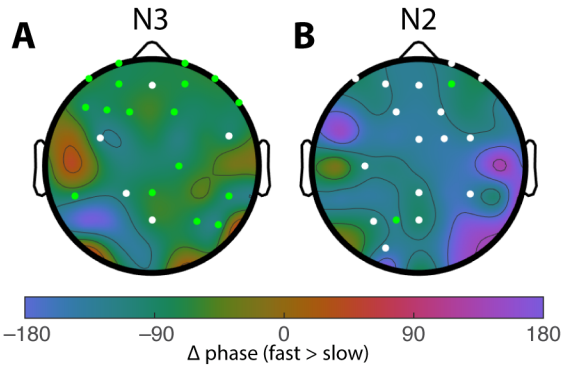

Figure 5. Differences in coupling phase between fast and slow spindle activity. Fast spindles occur ~90° earlier than slow spindles in both N3 (A) and N2 (B). Colored circles indicate electrodes showing significant phase differences across subjects after FDR correction (green) or uncorrected (white).

Combined, these findings (which were similar for Night 2) indicate that fast and slow spindle activity are tied to different phases of the local SO cycle, but also that N2 and N3 SOs coordinate spindle activity in subtly different ways.

Regional differences in coupling phase

While the preceding analyses demonstrated relatively consistent coupling phases across the scalp for all combinations of spindle class and sleep stage, the circular distributions of Fig. 4A (insets) also indicate substantial between-channel variability. To determine if there was any systematic pattern to this, we assigned channels to one of three regions (anterior, central, posterior; Fig. 6, inset) and averaged coupling phases across channels in each region for each subject. The resulting distributions were all significantly non-uniform (all $P_{corr}<0.05$), indicating consistent group-level clustering of coupling phase within each region for each condition). Also visible in these plots are the previously identified differences in coupling phase across conditions. Considering regional differences, N3 spindles appeared to peak around 25° later in the SO cycle in anterior compared to central and posterior regions (Fig. 6AC), while no differences were apparent during N2 (Fig. 6BD). To evaluate these observations statistically, we determined interregional phase differences separately for each subject to account for

individual differences not captured by the group-level approach of Fig. 6, and compared the resulting values to zero (one-sample t tests). These analyses confirmed that anterior N3 spindles occurred significantly later in the SO cycle compared to central (for fast and slow spindles) and posterior (for fast spindles) areas, although these analyses did not survive multiple comparison correction (detailed statistics in Table 2). However, analyses from night 2 confirmed the anterior vs. central difference for both fast and slow N3 spindles, thus suggesting subtle regional differences regarding the SO phase of maximal spindle expression.

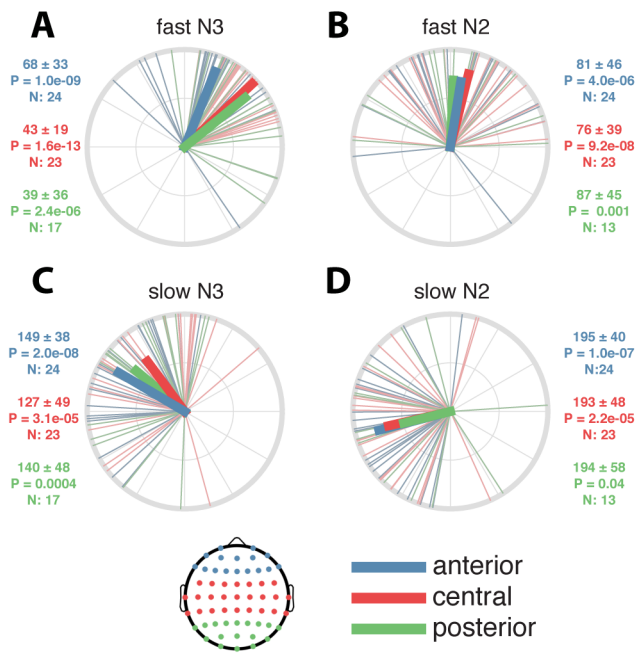

Figure 6. Regional differences in coupling phase. Numbers next to each circular plot indicate mean phase (± SD), P value (uncorrected) of Rayleigh test for non-uniformity, and number of included subjects. Inset: topography showing assignment of channels to regions.

	anterior vs. central			anterior vs. posterior			central vs. posterior		
	mean ± SD	P	N	mean ± SD	P	N	mean ± SD	P	N
N3 fast	**24 ± 36 ***	**0.01**	**24**	**31 ± 38**	**0.04**	**18**	5 ± 34 *	0.50	18
N2 fast	7 ± 39	0.65	23	3 ± 35	0.90	13	–18 ± 49	0.25	13
N3 slow	**26 ± 44 ***	**0.005**	**24**	19 ± 61	0.72	18	–1 ± 60 *	0.77	18
N2 slow	6 ± 47	0.80	23	–5 ± 62	0.34	13	9 ± 62 *	0.38	13

Table 2. Regional differences in coupling phase. Indicated are mean phase difference (± SD), P value (uncorrected) of one-sample t test vs. zero, and number of included subjects. Note that for these analyses, subjects are included only when they have ≥ 20 SOs on at least one electrode in each of the compared regions. Bold entries: significant phase difference on night 1 (shown in Fig. 6). Asterisks: significant phase difference on night 2.

Individual differences in coupling phase are stable across nights

Beside regional differences in coupling phase, the circular plots of Fig. 4 (right) and Fig. 6 also indicate substantial individual differences in the exact phase of coupling. To further examine this phenomenon, we analyzed the distribution of coupling phases across channels within subjects. As illustrated in the top row of Fig. 7 for two sample subjects, both individuals showed highly non-uniform distributions across channels with fast spindles (Fig. 7A) most prominent preceding, and slow spindles (Fig. 7B) following the SO peak. However, coupling phases clearly differed between these individuals, for both fast and slow spindles. Interestingly, plotting the same subjects' phase distributions for their second night indicated that individual differences in coupling phase are consistent across nights (Fig. 7AB, bottom), raising the possibility that this variability constitutes a stable trait.

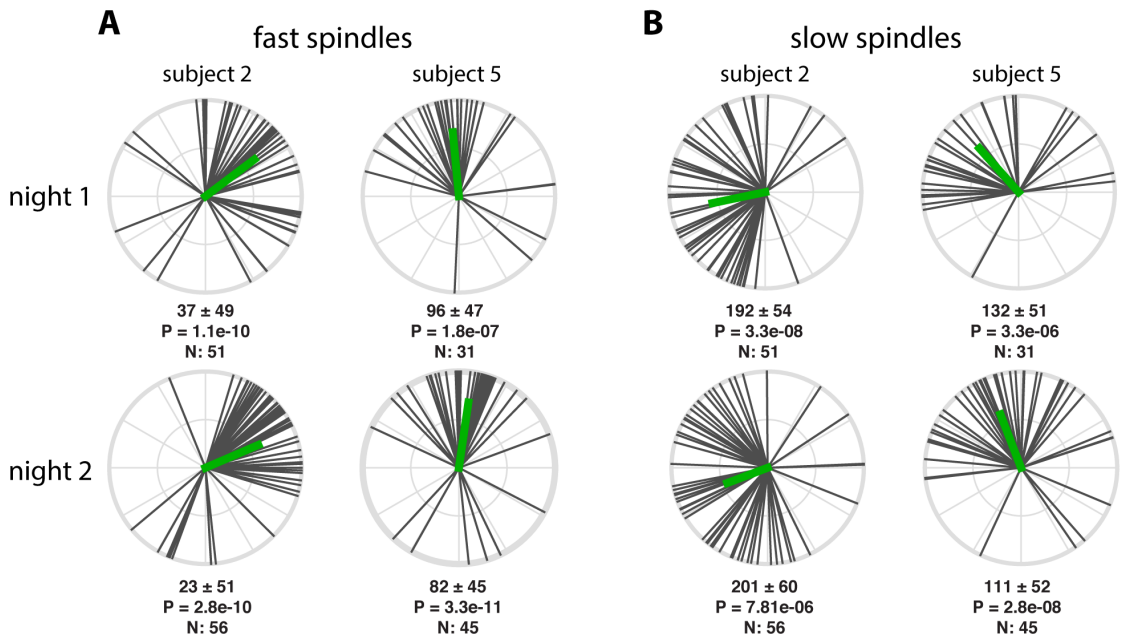

Figure 7. Individual variability of N3 coupling phases for two example subjects. Numbers below each circular plot indicate mean phase across channels (± SD), P value (uncorrected) of circular tests for non-uniformity, and number of included electrodes

To further examine this notion, we used circular correlation techniques to determine if there is a reliable association between subjects' coupling phases across nights. Given the general consistency of coupling phases across channels, we first averaged coupling phases across all available channels for each subject. Using this approach, we obtained remarkably strong cross-night correlations of coupling phase in each condition (all $P_{corr}<0.04$), indicating that individuals who express spindles in a later SO phase in one night tend to show the same pattern in the next night (Fig. 8). This was the case even for fast N3 spindles, where strong group-level clustering left relatively little between-subject variance (phases night 1: 52 ± 19°; span: 92°). In contrast, between-subject phase variability was much greater for fast N2 spindles (79 ± 46°; span:

203°), and slow spindles in both N3 and N2 (N3: 141 ± 35°; span: 153°; N2: 194 ± 36° span: 162°), spanning approximately half of the SO cycle. Thus, some subjects express spindles in an SO phase that deviates substantially from the group average, but they do so consistently across nights. We did not find evidence that coupling dynamics differed between the two nights (one-sample t tests of within-subject phase differences vs. zero: all P>0.18), suggesting that there were no task-induced alterations of SO-spindle coupling dynamics.

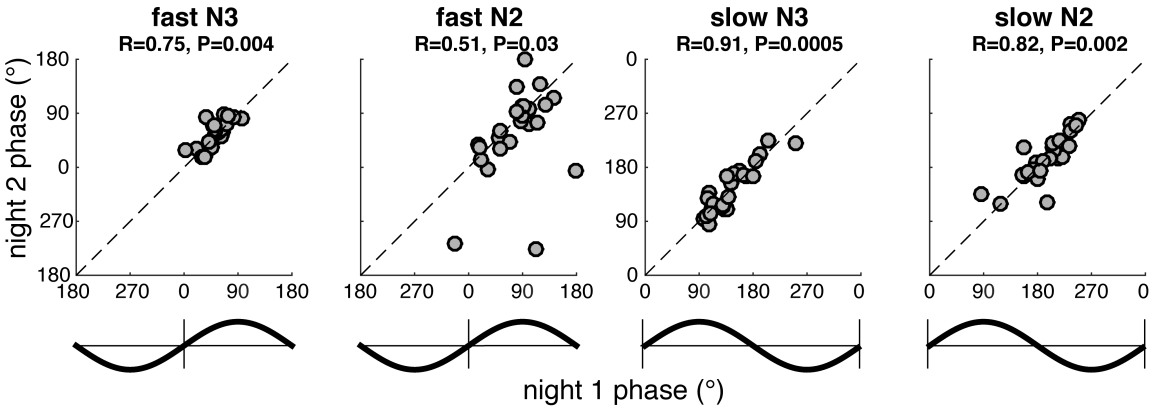

Figure 8. Stable individual differences of global SO-spindle coupling phase. Each scatter plot shows individuals' preferred coupling phases for nights 1 (x-axis) and 2 (y-axis). Each individual's coupling phase estimates are averaged across all available electrodes. Correlation coefficients (R) and (uncorrected) P values from circular correlation analyses are indicated above each plot. Note the different axis scales for fast and slow spindles, also indicated by schematic SO waveforms. Also note that because of the circular nature of phase estimates, data points close to the edge "wrap around" and are also close to the opposite side.

Cross-night stability of regional SO-spindle coupling

Given that we observed non-negligible regional variability of coupling phases within subjects (Fig. 6; Table 1), we repeated the preceding cross-night correlations separately for anterior, central, and posterior regions (Fig. 9). These analyses indicated that individual differences in coupling phase were significantly correlated across nights in anterior and central regions for three out of four conditions (all P_{corr}<0.05), with the remaining correlations showing trends to significance. In contrast, posterior coupling phases showed a significant correlation only for fast N3 spindles, although this association did not survive correction for multiple comparisons. However, we emphasize that an absence of significant cross-night correlations in posterior areas does not imply that spindles are not consistently coordinated by the regional SO cycle, only that there is more night-to-night variability within subjects. This observation may be related the smaller number of detected SOs and included subjects for posterior analyses. Also note how observations are clustered into different SO phases for different regions, spindle classes and sleep stages, consistent with the observations presented in previous sections.

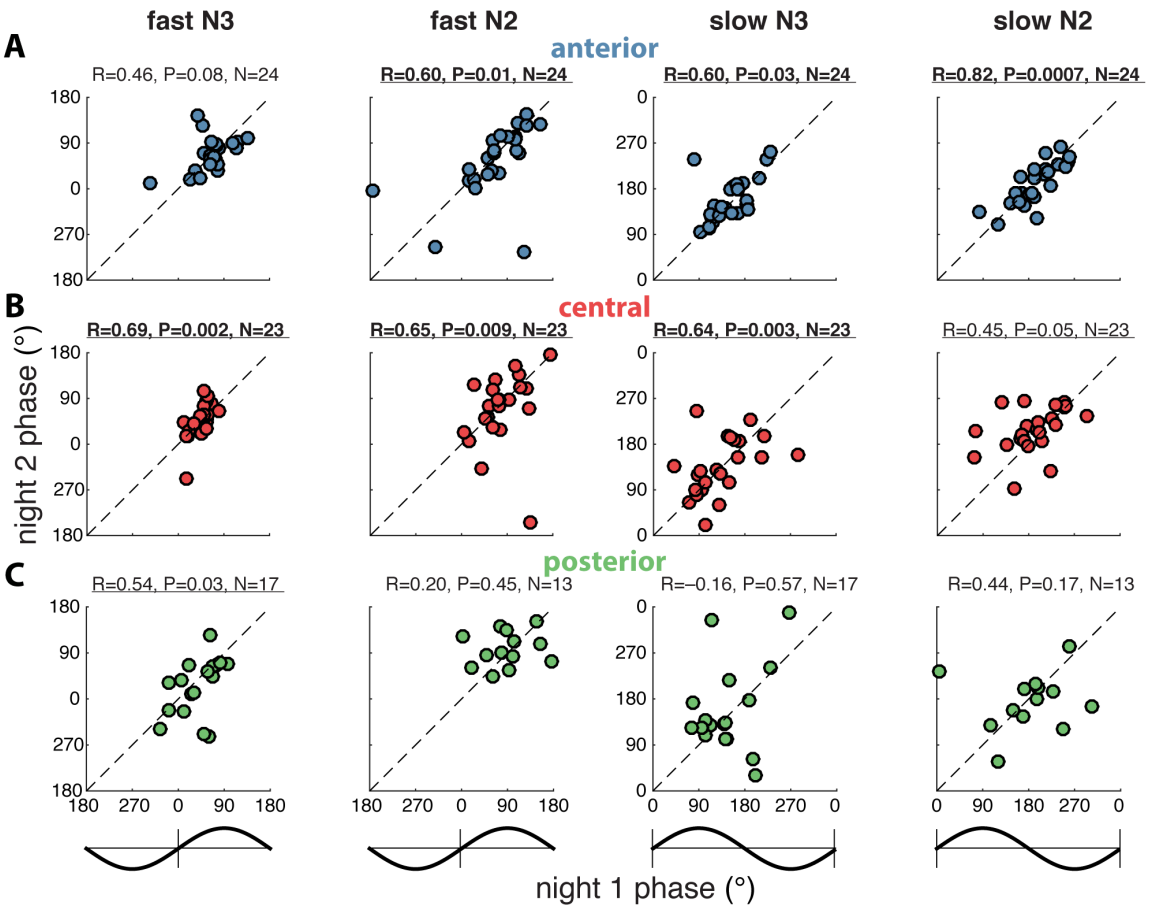

Figure 9. Stable individual differences of regional SO-spindle coupling phase. Figure layout as in Fig. 8, only with coupling phases averaged separately across available anterior (A), central (B), and posterior electrodes (C). Number of included subjects (N) indicated above each plot. Note that for these analyses, subjects are included only when they have ≥ 20 SOs on at least one electrode in the analyzed region in both nights. Significant (P<0.05, uncorrected) correlations are underlined, and correlations surviving multiple comparison correction are indicated in bold.

SO-spindle coupling and memory

Given previous reports that SO-spindle dynamics may be predictive of overnight memory retention (Niknazar et al., 2015; Demanuele et al., 2017; Helfrich et al., 2017), we explored whether individual variability in coupling phase on the learning night is associated with procedural memory change. Individuals showed significant improvement in the number of correctly completed motor sequences on the MST (16.3 ± 12.6%; t(23)=6.4, $P<10^{-5}$), consistent with typical overnight gains in healthy subjects (Walker et al., 2002; Manoach et al., 2004; Wamsley et al., 2013; Demanuele et al., 2017). However, we did not observe reliable associations between the SO phase of preferential spindle expression and memory improvement, for either fast or slow spindles, in either N3 or N2 sleep, and using either global or regional estimates of coupling phase (circular-linear correlation analyses: all P>0.11).

Discussion

The current study addresses the large-scale dynamics of SO-spindle coupling. Our main findings are that 1) local spindle activity is coupled to the local SO phase; 2) spindles are preferentially expressed in distinct phases of the SO cycle as a function of a) spindle class (slow vs. fast); b) sleep stage; and c) cortical region; and 3) individual differences in coupling phase are stable across nights.

We found that the phase of locally detected SOs robustly orchestrates local spindle activity at virtually every electrode and across all combinations of spindle class and sleep stage (Table 1), extending earlier evidence of regionally restricted spindle modulation by the local SO phase (Cox et al., 2014c). These findings are relevant to theories that SO-spindle coupling facilitates the recoding of temporary memory traces to more permanent cortical representations (Rasch and Born, 2013; Bergmann and Staresina, 2017). Specifically, the demonstration that local SO-spindle coupling extends across the cortex adds an important spatial component to this temporal coordination, providing the neurophysiological prerequisite for circuit-specific plasticity processes and the consolidation of specific memory traces (Huber et al., 2004, 2006; Cox et al., 2014a; Yordanova et al., 2017).

Regarding the precise SO phase of maximal spindle activity, we observed both known and novel sources of variability in coupling dynamics. First, our findings confirm the general dissociation of fast and slow spindle activity, with fast spindles having maximal amplitude preceding, and slow spindles following, the SO peak (Mölle et al., 2011; Cox et al., 2014c; Klinzing et al., 2016; Yordanova et al., 2017). This phenomenon was observed across the scalp for both N3 and N2 (Fig. 4), with fast spindles occurring approximately a quarter of a cycle earlier, most robustly in anterior areas (Fig. 5). These findings add to accumulating evidence that fast and slow spindles reflect distinct phenomena (Schabus et al., 2007; Ayoub et al., 2013; D'Atri et al., 2017; Purcell et al., 2017), and indicate that while these oscillations show distinct topographical patterns (Werth et al., 1997; Zeitlhofer et al., 1997; Cox et al., 2017), spindle activity is modulated by the SO cycle even at sites where they are less prominent.

Second, coupling phase differed between sleep stages. Slow spindles occurred significantly later (i.e., 45° closer to the SO trough) in N2 than N3, while for fast spindles there were no significant differences. Third, we observed subtle, but consistent regional differences in the phase of spindle expression (Fig. 6; Table 2). In particular, N3 spindles occurred ~25° later in the SO cycle in anterior vs. central regions, for both spindle classes. Although it is presently unclear what underlies these regional and stage differences, these factors are important to consider when the precise coupling phase is the focus of attention.

Beside systematic group-level variability, we found remarkably large individual differences in the preferred phase of spindle expression that, depending on condition,

spanned up to half of the SO cycle, thereby attenuating group effects (e.g., non-significant group-level clustering of slow spindles: Fig. 4CD). Intriguingly, this variability was highly stable within subjects across nights (Fig. 8), and even observed within cortical regions (Fig. 9). Several features of SO (Massimini et al., 2004) and spindle activity (De Gennaro et al., 2005; Ujma et al., 2015; Cox et al., 2017) show large yet reproducible individual differences related to underlying variability in anatomy (Piantoni et al., 2013b). From this perspective, the fingerprint-like nature of SO-spindle coupling is perhaps not entirely surprising. However, previous reports correlating coupling phase to memory change rely on the implicit assumption that coupling phase is a state-like phenomenon in which individual differences are exclusively related to consolidation of recently encoded information. In contrast, our results indicate that any observed relation between coupling phase and behavior may reflect a general trait, rather than a task-induced phenomenon, similar to other trait-like relations between sleep physiology and cognitive ability (Bódizs et al., 2005; Schabus et al., 2006; Lustenberger et al., 2012; Lerner et al., 2016). Consistent with this notion, we found no differences in the SO phase of maximal spindle activity between the baseline and learning nights.

Overnight MST performance improvements were consistent with prior studies (Walker et al., 2002; Manoach et al., 2004; Wamsley et al., 2013; Demanuele et al., 2017). However, we did not find any link between coupling phase and memory change. Several recent studies suggest that whether coupling phase is related to memory change depends on a number of factors including the task, population and the use of pharmacological intervention (Niknazar et al., 2015; Demanuele et al., 2017; Helfrich et al., 2017). It remains to be seen under what conditions coupling phase mediates memory consolidation.

SO densities varied considerably across the scalp (Fig. 2A), resulting in both noisier within-subject coupling estimates and smaller sample sizes in regions with fewer SOs (Fig. 2D), potentially explaining the weaker effects in posterior regions. While fewer SOs could be interpreted as less robust SO-spindle coupling, we assessed coupling for individually detected SOs to avoid this confounding influence. Thus, while the likelihood of observing SOs clearly varies across the scalp, whenever and wherever they are detected, SOs robustly organize the expression of local spindle activity.

SO-spindle coupling was determined separately at each of 58 electrodes, contrasting with studies assessing coupling on a limited number of channels (Mölle et al., 2011; Piantoni et al., 2013a; Demanuele et al., 2017), and with approaches where multi-channel spindle activity is related to the SO phase from a single (virtual) channel (Mölle et al., 2011; Klinzing et al., 2016; Yordanova et al., 2017). The latter approach assumes that SOs are relatively global events that are synchronized across the scalp. However, our analyses of SO co-occurrence (≤400 ms) indicate that the average SO involves fewer than ten channels, consistent with invasive findings (Nir et al., 2011). Counting only SOs that co-occur with minimal phase shifts (≤100 ms; Fig. 2C, 3) resulted in a 40-45% reduction in channel involvement, further arguing against SOs as a uniform,

zero phase-lag phenomenon. Such phase shifts are also consistent with evidence of SOs propagating across the cortex (Massimini et al., 2004; Murphy et al., 2009; Nir et al., 2011).

Local EEG dynamics were accentuated with the surface Laplacian (Perrin et al., 1989; Tenke and Kayser, 2005). While it might be argued that this approach suppresses true global SO (and spindle) activity, available evidence suggests that the Laplacian results in no loss of global information (Tenke et al., 2015). More importantly, both invasive (Andrillon et al., 2011; Nir et al., 2011; Piantoni et al., 2016) and EEG [(Massimini et al., 2004; Cox et al., 2014c); Fig. 1] evidence indicates that SOs and spindles have important local components, strongly favoring an approach sensitive to such features. We speculate that the more global appearance of SOs in spatially unfiltered EEG recordings is largely due to volume conduction, ensuring that large-amplitude frontal SOs are detected at distant sites.

We assessed coupling between SOs and continuous fluctuations in sigma power rather than individually detected sleep spindles. Because the spatiotemporal properties of SO-sigma coupling are relatively similar in the presence and absence of discrete spindles (Klinzing et al., 2016), the analysis of continuous sigma activity arguably offers a more comprehensive perspective on coupling dynamics. Nonetheless, our results are in line with reports based on discrete spindle detection (Mölle et al., 2011; Klinzing et al., 2016; Demanuele et al., 2017; Helfrich et al., 2017), suggesting that this methodological choice does not pose a major concern.

Finally, we emphasize that examinations of preferred coupling phase only partially capture the dynamics of coupled sleep oscillations. Even when considering a single channel for a single subject, we have anecdotally observed that algorithmically detected spindles (1) reach their maximum amplitude in highly variable SO phases; (2) span a substantial portion or even the entire cycle of the SO waveform; or (3) may not be associated with any SO at all, most commonly during N2. Conversely, not all SOs are associated with discrete spindles. Given both our main findings and these additional complexities, we caution against the overly simplistic conceptualization that spindle activity is rigidly tied to a single SO phase. Still, spindle activity occurring in a narrow SO phase may induce plasticity more effectively (Latchoumane et al., 2017), raising the possibility that the optimal phase could be different for different individuals and cortical regions. This suggestion may also be of practical relevance to closed-loop approaches targeting stimulus delivery at a specific SO phase (Ngo et al., 2013; Cox et al., 2014b; Santostasi et al., 2015).

In summary, we have identified systematic differences in the preferred SO phase of spindle expression as a function of spindle class, cortical region, sleep stage, and individual. While the causes and consequences of these many sources of variability remain to be determined, we suggest that locally coordinated oscillatory rhythms offer the sleeping brain a vast repertoire of building blocks to flexibly process, consolidate,

and reorganize experiences encoded within and across brain structures, with important functional and clinical implications.

Conflict of Interest

The authors declare no competing financial interests.

Acknowledgements

This work was supported by grants from The Netherlands Organization for Scientific Research (NWO) to RC (446-14-009); National Institutes of Health to RS (MH048832), DSM (Manoach) (K24MH099421), RS and DSM (Manoach) (MH092638); George and Marie Vergottis Postdoctoral Fellowship to DSM (Mylonas); The Harvard Clinical and Translational Science Center (TR001102); and Stanley Center for Psychiatric Research at Broad Institute.

References

Andrillon T, Nir Y, Staba RJ, Ferrarelli F, Cirelli C, Tononi G, Fried I (2011) Sleep Spindles in Humans: Insights from Intracranial EEG and Unit Recordings. J Neurosci 31:17821–17834.

Ayoub A, Aumann D, Hörschelmann A, Kouchekmanesch A, Paul P, Born J, Marshall L (2013) Differential effects on fast and slow spindle activity, and the sleep slow oscillation in humans with carbamazepine and flunarizine to antagonize voltage-dependent Na+ and Ca2+ channel activity. Sleep 36:905–911.

Barakat M, Doyon J, Debas K, Vandewalle G, Morin A, Poirier G, Martin N, Lafortune M, Karni A, Ungerleider LG, Benali H, Carrier J (2011) Fast and slow spindle involvement in the consolidation of a new motor sequence. Behav Brain Res 217:117–121.

Benjamini Y, Hochberg Y (1995) Controlling the false discovery rate: a practical and powerful approach to multiple testing. J R Stat Soc 57:289–300.

Berens P (2009) CircStat: A MATLAB toolbox for circular statistics. J Stat Softw 31:1–21.

Bergmann TO, Staresina BP (2017) Neuronal Oscillations and Reactivation Subserving Memory Consolidation. In: Cognitive Neuroscience of Memory Consolidation, pp 185–207.

Bódizs R, Kis T, Lázár AS, Havrán L, Rigó P, Clemens Z, Halász P (2005) Prediction of general mental ability based on neural oscillation measures of sleep. J Sleep Res 14:285–292.

Canolty RT, Edwards E, Dalal SS, Soltani M, Nagarajan SS, Kirsch HE, Berger MS, Barbaro NM, Knight RT (2006) High gamma power is phase-locked to theta oscillations in human neocortex. Science (80-) 313:1626–1628.

Canolty RT, Knight RT (2010) The functional role of cross-frequency coupling. Trends Cogn Sci 14:506–515.

Cash SS, Halgren E, Dehghani N, Rossetti AO, Thesen T, Wang C, Devinsky O, Kuzniecky R, Doyle W, Madsen JR, Bromfield E, Eross L, Halasz P, Karmos G, Csercsa R, Wittner L, Ulbert I (2009) The Human K-Complex Represents an Isolated Cortical Down-State. Science (80-) 324:1084–1087.

Cox R, Hofman WF, de Boer M, Talamini LM (2014a) Local sleep spindle modulations in relation to specific memory cues. Neuroimage 99:103–110.

Cox R, Hofman WF, Talamini LM (2012) Involvement of spindles in memory consolidation is slow wave sleep-specific. Learn Mem 19:264–267.

Cox R, Korjoukov I, de Boer M, Talamini LM (2014b) Sound Asleep: Processing and Retention of Slow Oscillation Phase-Targeted Stimuli Vyazovskiy V, ed. PLoS One 9:e101567.

Cox R, Schapiro AC, Manoach DS, Stickgold R (2017) Individual Differences in Frequency and Topography of Slow and Fast Sleep Spindles. Front Hum Neurosci 11.

Cox R, van Driel J, de Boer M, Talamini LM (2014c) Slow Oscillations during Sleep Coordinate Interregional Communication in Cortical Networks. J Neurosci 34:16890–16901.

D'Atri A, Novelli L, Ferrara M, Bruni O, De Gennaro L (2017) Different Maturational

Changes of Fast and Slow Sleep Spindles in The First Four Years of Life. Sleep Med 42:73–82.
De Gennaro L, Ferrara M (2003) Sleep spindles: an overview. Sleep Med Rev 7:423–440.
De Gennaro L, Ferrara M, Vecchio F, Curcio G, Bertini M (2005) An electroencephalographic fingerprint of human sleep. Neuroimage 26:114–122.
Delorme A, Makeig S (2004) EEGLAB: an open source toolbox for analysis of single-trial EEG dynamics including independent component analysis. J Neurosci Methods 134:9–21.
Demanuele C, Bartsch U, Baran B, Khan S, Vangel MG, Cox R, Hämäläinen M, Jones MW, Stickgold R, Manoach DS (2017) Coordination of Slow Waves With Sleep Spindles Predicts Sleep-Dependent Memory Consolidation in Schizophrenia. Sleep 40:369–465.
Ferrarelli F, Huber R, Peterson M, Massimini M, Murphy M, Riedner B, Watson A, Bria P, Tononi G (2007) Reduced sleep spindle activity in schizophrenia patients. Am J Psychiatry 164:483–492.
Fischer S, Nitschke MF, Melchert UH, Erdmann C, Born J (2005) Motor memory consolidation in sleep shapes more effective neuronal representations. J Neurosci 25:11248–11255.
Helfrich RF, Mander BA, Jagust WJ, Knight RT, Walker MP (2017) Old Brains Come Uncoupled in Sleep: Slow Wave-Spindle Synchrony, Brain Atrophy, and Forgetting. Neuron 97:1–10.
Huber R, Ghilardi MF, Massimini M, Ferrarelli F, Riedner BA, Peterson MJ, Tononi G (2006) Arm immobilization causes cortical plastic changes and locally decreases sleep slow wave activity. Nat Neurosci 9:1169–1176.
Huber R, Ghilardi MF, Massimini M, Tononi G (2004) Local sleep and learning. Nature 430:78–81.
Iber C, Ancoli-Israel S, Chesson A, Quan S (2007) The AASM manual for the scoring of sleep and associated events: rules, terminology and technical specifications. American Academy of Sleep Medicine.
Klinzing JG, Mölle M, Weber F, Supp G, Hipp JF, Engel AK, Born J (2016) Spindle activity phase-locked to sleep slow oscillations. Neuroimage 134:607–616.
Kurth S, Ringli M, Geiger A, LeBourgeois M, Jenni OG, Huber R (2010) Mapping of Cortical Activity in the First Two Decades of Life: A High-Density Sleep Electroencephalogram Study. J Neurosci 30:13211–13219.
Latchoumane C-F V., Ngo H-V V., Born J, Shin H-S (2017) Thalamic Spindles Promote Memory Formation during Sleep through Triple Phase-Locking of Cortical, Thalamic, and Hippocampal Rhythms. Neuron 95:424–435.e6.
Latreille V, Carrier J, Lafortune M, Postuma RB, Bertrand J-A, Panisset M, Chouinard S, Gagnon J-F (2015) Sleep spindles in Parkinson's disease may predict the development of dementia. Neurobiol Aging 36:1083–1090.
Lerner I, Lupkin SM, Corter JE, Peters SE, Cannella LA, Gluck MA (2016) The influence of sleep on emotional and cognitive processing is primarily trait- (but not state-) dependent. Neurobiol Learn Mem 134:275–286.
Lustenberger C, Maric A, Dürr R, Achermann P, Huber R (2012) Triangular Relationship

between Sleep Spindle Activity, General Cognitive Ability and the Efficiency of Declarative Learning. PLoS One 7.
Lüthi A (2013) Sleep Spindles Where They Come From, What They Do. Neurosci 20:243–256.
Makeig S, Jung T-P, Bell AJ, Ghahremani D, Sejnowski TJ (1997) Blind separation of auditory event-related brain responses into independent components. Proc Natl Acad Sci 94:10979–10984.
Mander BA, Rao V, Lu B, Saletin JM, Lindquist JR, Ancoli-Israel S, Jagust W, Walker MP (2013) Prefrontal atrophy, disrupted NREM slow waves and impaired hippocampal-dependent memory in aging. Nat Neurosci 16:357–364.
Manoach DS, Cain MS, Vangel MG, Khurana A, Goff DC, Stickgold R (2004) A failure of sleep-dependent procedural learning in chronic, medicated schizophrenia. Biol Psychiatry 56:951–956.
Marshall L, Helgadóttir H, Mölle M, Born J (2006) Boosting slow oscillations during sleep potentiates memory. Nature 444:610–613.
Massimini M, Huber R, Ferrarelli F, Hill S, Tononi G (2004) The sleep slow oscillation as a traveling wave. J Neurosci 24:6862–6870.
Mölle M, Bergmann TO, Marshall L, Born J (2011) Fast and Slow Spindles during the Sleep Slow Oscillation: Disparate Coalescence and Engagement in Memory Processing. Sleep 34:1411–1421.
Mölle M, Eschenko O, Gais S, Sara SJ, Born J (2009) The influence of learning on sleep slow oscillations and associated spindles and ripples in humans and rats. Eur J Neurosci 29:1071–1081.
Murphy M, Riedner BA, Huber R, Massimini M, Ferrarelli F, Tononi G (2009) Source modeling sleep slow waves. Proc Natl Acad Sci 106:1608–1613.
Ngo H-V V., Martinetz T, Born J, Mölle M (2013) Auditory Closed-Loop Stimulation of the Sleep Slow Oscillation Enhances Memory. Neuron 78:545–553.
Niknazar M, Krishnan GP, Bazhenov M, Mednick SC (2015) Coupling of Thalamocortical Sleep Oscillations Are Important for Memory Consolidation in Humans. PLoS One 10:e0144720.
Nir Y, Staba RJ, Andrillon T, Vyazovskiy V V., Cirelli C, Fried I, Tononi G (2011) Regional Slow Waves and Spindles in Human Sleep. Neuron 70:153–169.
Perrin F, Pernier J, Bertrand O, Echallier JF (1989) Spherical splines for scalp potential and current density mapping. Electroencephalogr Clin Neurophysiol 72:184–187.
Piantoni G, Astill RG, Raymann RJEM, Vis JC, Coppens JE, Van Someren EJW (2013a) Modulation of gamma and spindle-range power by slow oscillations in scalp sleep EEG of children. Int J Psychophysiol 89:252–258.
Piantoni G, Halgren E, Cash SS (2016) Spatiotemporal Characteristics of Sleep Spindles Depend on Cortical Location. Neuroimage 146:236–245.
Piantoni G, Poil S-S, Linkenkaer-Hansen K, Verweij IM, Ramautar JR, Van Someren EJW, Van Der Werf YD (2013b) Individual differences in white matter diffusion affect sleep oscillations. J Neurosci 33:227–233.
Plante DT, Goldstein MR, Landsness EC, Peterson MJ, Riedner BA, Ferrarelli F, Wanger T, Guokas JJ, Tononi G, Benca RM (2013) Topographic and sex-related differences in

sleep spindles in major depressive disorder: A high-density EEG investigation. J Affect Disord 146:120–125.
Purcell SM, Manoach DS, Demanuele C, Cade BE, Mariani S, Cox R, Panagiotaropoulou G, Saxena R, Pan JQ, Smoller JW, Redline S, Stickgold R (2017) Characterizing sleep spindles in 11,630 individuals from the National Sleep Research Resource. Nat Commun 8:15930.
Rasch B, Born J (2013) About sleep's role in memory. Physiol Rev 93:681–766.
Santostasi G, Malkani R, Riedner B, Bellesi M, Tononi G, Paller KA, Zee PC (2015) Phase-locked loop for precisely timed acoustic stimulation during sleep. J Neurosci Methods 259:101–114.
Schabus M, Dang-Vu TT, Albouy G, Balteau E, Boly M, Carrier J, Darsaud A, Degueldre C, Desseilles M, Gais S, Phillips C, Rauchs G, Schnakers C, Sterpenich V, Vandewalle G, Luxen A, Maquet P (2007) Hemodynamic cerebral correlates of sleep spindles during human non-rapid eye movement sleep. Proc Natl Acad Sci U S A 104:13164–13169.
Schabus M, Hödlmoser K, Gruber G, Sauter C, Anderer P, Klösch G, Parapatics S, Saletu B, Klimesch W, Zeitlhofer J (2006) Sleep spindle-related activity in the human EEG and its relation to general cognitive and learning abilities. Eur J Neurosci 23:1738–1746.
Steriade M, Domich L, Oakson G, Deschenes M (1987) The deafferented reticular thalamic nucleus generates spindle rhythmicity. J Neurophysiol 57:260–273.
Steriade M, Nunez A, Amzica F, Nuñez a, Amzica F, Nunez A, Amzica F (1993) A novel slow (< 1 Hz) oscillation of neocortical neurons in vivo: depolarizing and hyperpolarizing components. J Neurosci 13:3252–3265.
Tenke CE, Kayser J (2005) Reference-free quantification of EEG spectra: combining current source density (CSD) and frequency principal components analysis (fPCA). Clin Neurophysiol 116:2826–2846.
Tenke CE, Kayser J, Abraham K, Alvarenga JE, Bruder GE (2015) Posterior EEG alpha at rest and during task performance: Comparison of current source density and field potential measures. Int J Psychophysiol 97:299–309.
Ujma PP, Gombos F, Genzel L, Konrad BN, Simor P, Steiger A, Dresler M, BÃ³dizs R (2015) A comparison of two sleep spindle detection methods based on all night averages: individually adjusted vs. fixed frequencies. Front Hum Neurosci 9:1–11.
van Driel J, Cox R, Cohen MX (2015) Phase-clustering bias in phase–amplitude cross-frequency coupling and its removal. J Neurosci Methods 254:60–72.
Walker MP, Brakefield T, Morgan A, Hobson JA, Stickgold R (2002) Practice with sleep makes perfect: Sleep-dependent motor skill learning. Neuron 35:205–211.
Wamsley EJ, Shinn AK, Tucker MA, Ono KE, McKinley SK, Ely A V, Goff DC, Stickgold R, Manoach DS (2013) The effects of eszopiclone on sleep spindles and memory consolidation in schizophrenia: a randomized placebo-controlled trial. Sleep 36:1369–1376.
Wamsley EJ, Tucker MA, Shinn AK, Ono KE, McKinley SK, Ely A V, Goff DC, Stickgold R, Manoach DS (2012) Reduced sleep spindles and spindle coherence in schizophrenia: mechanisms of impaired memory consolidation? Biol Psychiatry

71:154–161.
Werth E, Achermann P, Dijk DJ, Borbély AA (1997) Spindle frequency activity in the sleep EEG: Individual differences and topographic distribution. Electroencephalogr Clin Neurophysiol 103:535–542.
Yordanova J, Kirov R, Verleger R, Kolev V (2017) Dynamic coupling between slow waves and sleep spindles during slow wave sleep in humans is modulated by functional pre-sleep activation. Sci Rep 7:14496.
Zeitlhofer J, Gruber G, Anderer P, Asenbaum S, Schimicek P, Saletu B (1997) Topographic distribution of sleep spindles in young healthy subjects. J Sleep Res 6:149–155.